Energy Storage and Saving 2 (2023) 487–494

Contents lists available at ScienceDirect

Energy Storage and Saving

journal homepage: http://www.keaipublishing.com/en/journals/energy-storage-and-saving/

Original article

Comparative study on heat transfer enhancement of metal foam and fins in a shell-and-tube latent heat thermal energy storage unit

Shuai Zhang [a], Ziyuan Li [b], Yuying Yan [a,*], Mark Alston [a], Limei Tian [b]

[a] Faculty of Engineering, University of Nottingham, University Park, Nottingham, NG7 2RD, UK
[b] Key Laboratory of Bionic Engineering (Ministry of Education), Jilin University, Changchun, 130022, China

ARTICLE INFO

Keywords:
Comparative study
Metal foam and fin
Thermal energy storage
Shell-and-tube heat storage unit
Melting front

ABSTRACT

Metal foam and fins are two popular structures that are employed to enhance the heat transfer of phase change materials in shell-and-tube heat storage units. However, it remains unclear which structure is better in terms of energy storage performance. In this study, the heat transfer enhancement performances of metal foam and fins are compared to provide guidance on the optimal structure to be chosen for practical applications. Three fin structures (four fins, two vertical fins, and two horizontal fins) are considered. Under the full configuration (volume fraction of metal = 3%), the unit with four fins was found to have a faster melting rate than those with vertical or horizontal fins. In other words, increasing the number of fins helps to accelerate the melting process. Nevertheless, the unit with metal foam enhancement has the highest melting rate. Under the half configuration (volume fraction of metal = 1.5%), the melting rate of the unit enhanced by metal foam is significantly decreased, whereas there is no remarkable changes in the units enhanced by fins. However, metal foam is still shown to be the best thermal enhancer. The energy storage rate of the unit enhanced by metal foam can be up to 10 times higher than that of the unit enhanced by fins.

1. Introduction

Thermal energy storage (TES) technology is a promising solution to improving the utilization efficiency in solar thermal applications and industrial waste heat recovery [1,2]. It enables the storage of surplus thermal energy, and releases it for subsequent use, which addresses the temporal mismatch between energy supply and demand. This is a very important functionality as solar energy is unsteady and intermittent. Moreover, the storage media can be transported to the user side so that thermal energy can be recovered and used in different locations. Industries are usually far away from residential buildings; in such cases, TES provides a useful approach to the recovery and use of industrial waste heat. Latent heat thermal energy storage (LHTES) has a large energy density and almost constant temperature during charging/discharging, which makes it an attractive technology [3–5]. However, the storage media, i.e., phase change materials (PCMs), commonly suffer from low thermal conductivity, leading to low melting and solidification rate. Hence, the energy storage efficiency requirement is not easily met [6].

The shell-and-tube heat storage unit is a popular device for TES [7]. In this unit, the annular space between the shell and the tube is filled with PCMs. The heat transfer fluid (HTF) exchanges heat with the PCM through the tube. The HTF and PCM are not in contact; hence, there is no risk of leakage of PCMs [8,9]. Many methods have been proposed to enhance the heat transfer in the shell-and-tube unit; they can generally be classified as those using porous skeletons, fins, particles, and heat pipes. Among the options, metal foam and fins are two popular structures owing to their excellent performance and ease of installation.

With metal foam, the porosity and pore size are two key factors. Liu et al. [10] performed a numerical study on the thermal performance of a shell-and-tube unit, where copper foam acts as the thermal enhancement structure and paraffin as the PCM. They analyzed the influence of the pore size and porosity of metal foam on the energy storage performance. Porosity was found to have a significant effect, while the influence of the pore size was smaller. Yang et al. [11] designed gradient pore structures for a vertical paraffin/copper foam LHTES unit. The copper foam with different pore configurations was placed in the upper, middle, and lower parts to form the gradient pore structure. They found that the positive gradient, i.e., decreasing porosity from top to bottom, had a better performance. Moreover, they found that although the positive gradient in the pore size increases the temperature uniformity, the pore size has a very limited influence on the melting process. The HTF is another important factor. Yang et al. [12] experimentally investigated the charging process of a vertical paraffin/copper foam LHTES unit. Hot water was used as the HTF, and the effect of the HTF velocity was analyzed. Copper foam was found to reduce the overall melting time by 64%. The HTF velocity has little influence on the melting rate of both paraffin/copper composite and pure paraffin. The role of metal foam in the charging and

Peer review under responsibility of Xi'an Jiaotong University.
* Corresponding author.
E-mail address: Yuying.Yan@nottingham.ac.uk (Y. Yan).

https://doi.org/10.1016/j.enss.2023.03.004
Received 23 November 2022; Received in revised form 24 March 2023; Accepted 31 March 2023
Available online 1 April 2023

Nomenclature

A_{mushy}	Mushy zone constant
ε	Porosity
ρ	Density
μ	Dynamic viscosity
β	Coefficient of thermal expansion
c_p	Specific heat capacity
f_l	Melting fraction of the entire phase change material (PCM)
h_v	Volumetric interfacial heat transfer coefficient
k	Thermal conductivity
m	Mass
K	Permeability
L	Latent heat
Nu	Nusselt number
p	Pressure
PPI	Pores per inch
t	Time
T	Temperature
VF	Volume fraction of copper
κ_{tor}, d_{fp}, d_{fs}	Variables used in predicting the permeability and inertia coefficient

discharging processes was explored by Fleming et al. [13]. They found that the enhancement ability of metal foam was greater for the charging process than for the discharging process.

The fin is another popular thermal enhancer that is used in the shell-and-tube unit. Longitudinal fins and radial fins are common types of fins. Dekhil et al. [14] compared the enhancement performance of longitudinal and radial fins. They found that fins significantly improve the melting and solidification rates, and longitudinal fins have superior performance than their radial counterparts. Some novel fins have been proposed recently, such as topology-optimized fins, tree-shaped fins, and ladder-shaped fins. Ge et al. [15] designed different topology-optimized fins and analyzed their thermal and economic performance. They concluded that optimized fins had the best thermal enhancement performance, and were cost-effective when the unit price ratio was less than 6. Zhang et al. [16] introduced tree-shaped fins. Their results indicate that the tree-fin heat storage unit has a fast solidification rate, excellent temperature uniformity, and a high energy discharge rate. Compared to the conventional radial-fin unit, the total solidification time is reduced by 66%. Liu et al. [17] proposed ladder-shaped fins to accelerate the melting process. They found that the fin angle has a significant impact on the melting process. Vertical and horizontal fins have a reduced melting time compared to the ones that are turned 45° from the vertical axis.

Metal foam and fins are two widely used structures to improve energy storage efficiency. However, it remains unclear which one is better. Very few studies have compared the performance of the two structures in the shell-and-tube unit, which makes choosing the better one for practical applications difficult. In the current research, the heat transfer enhancement performance of metal foam and fins was compared. Three fin structures (horizontal-vertical fins, vertical fins, and horizontal fins) and two metal configurations (volume fraction of metal = 3% and 1.5%) were considered. The melting rate, solid-liquid phase field, energy storage rate, etc. are analyzed. This study aims to provide guidance on choosing a superior enhancement structure for TES applications.

2. Numerical model

2.1. Physical and mathematical models

The physical models of metal foam- and fin-enhanced heat storage units are shown in Fig. 1. Copper foam has a porosity of 0.97; hence, in case 1 where the copper foam fills in the heat storage unit, the volume fraction (VF) of copper is 3%. In cases 2–4, the VF is also 3%. These cases are referred to as the "full configuration". In case 2, fins are arranged horizontally and vertically; the thickness and length are 3 mm and 25.1 mm, respectively (Table 1). In case 3, two fins are arranged vertically; the length is the same, while the thickness is 6 mm. In case 4, two fins with the same thickness and length as case 3 are arranged horizontally.

Table 1
Parameters of 8 cases used in the current study.

Parameter	Case 1	Case 2	Case 3	Case 4	Case 5	Case 6	Case 7	Case 8
Foam porosity	0.970	-	-	-	0.985	-	-	-
Fin length (mm)	-	25.1	25.1	25.1	-	25.1	25.1	25.1
Fin thickness (mm)	-	3.0	6.0	6.0	-	1.5	3.0	3.0

Table 2
Thermo-physical properties of paraffin and copper [18].

Material	Property	Value
Paraffin	ρ	0.785 g·cm^{-3}
	L	175.2 J·g^{-1}
	T_m	54.4 °C – 64.1 °C
	c_p	2.85 kJ·kg^{-1}·K^{-1}
	k	0.30 W·m^{-1}·K^{-1} (solid)
		0.10 W·m^{-1}·K^{-1} (liquid)
	μ	3.65 mPa·s
	β	3.085 ×10^{-4} K^{-1}
Copper	ρ	8.92 g·cm^{-3}
	c_p	0.38 kJ·kg^{-1}·K^{-1}
	k	401 W·m^{-1}·K^{-1}

As the cost of copper is high, the enhancement structure in small quantities is sometimes employed to minimize cost. In cases 5–8, the volume fraction of copper is reduced to 1.5%, which is half the corresponding value in cases 1–4. These cases are referred to as the "half configuration". In case 5, copper foam has a porosity of 0.985. In cases 6–8, the fin thickness values are half the corresponding values in cases 2–4.

A two-dimensional (2D) model was employed because the variation along the axis is insignificant within a limited length. Some assumptions were made for the numerical model: (1) Thermo-physical properties are independent of temperature (Table 2 [18]); (2) liquid PCM is laminar and incompressible; (3) PCM and copper foam are isotropic and homogenous; (4) Boussinesq approximation is used to deal with natural convection.

The continuity equation is given by [19]:

$$\nabla \cdot \vec{U} = 0 \tag{1}$$

Momentum equations for the PCM/fin configuration are as follows [20,21]:

$$\rho_{PCM}\frac{\partial u}{\partial t}+\rho_{PCM}\left(\vec{U}\cdot\nabla u\right) = -\frac{\partial p}{\partial x} + \mu_{PCM}\nabla^2 u - \frac{(1-\varphi)^2}{(\varphi^3+\omega)}A_{mushy}u \tag{2}$$

$$\rho_{PCM}\frac{\partial v}{\partial t}+\rho_{PCM}\left(\vec{U}\cdot\nabla v\right) = -\frac{\partial p}{\partial y}+\mu_{PCM}\nabla^2 v+\rho_{PCM}\,g\,\beta\left(T-T_{m1}\right)-\frac{(1-\varphi)^2}{(\varphi^3+\omega)}A_{mushy}v \tag{3}$$

where ρ_{PCM} is the PCM density; β is the thermal expansion coefficient; μ_{PCM} is the viscosity; and φ is the melting fraction [20]:

$$\varphi=\frac{T-T_{m1}}{T_{mu}-T_{ml}}=\begin{cases}0 & \text{for T} < T_{m1}\\ 0-1 & \text{for } T_{m1} \le \text{T} \le T_{mu}\\ 1 & \text{for T} > T_{mu}\end{cases} \tag{4}$$

where T_{ml} and T_{mu} are respectively the solidus temperature and liquidus temperature of paraffin.

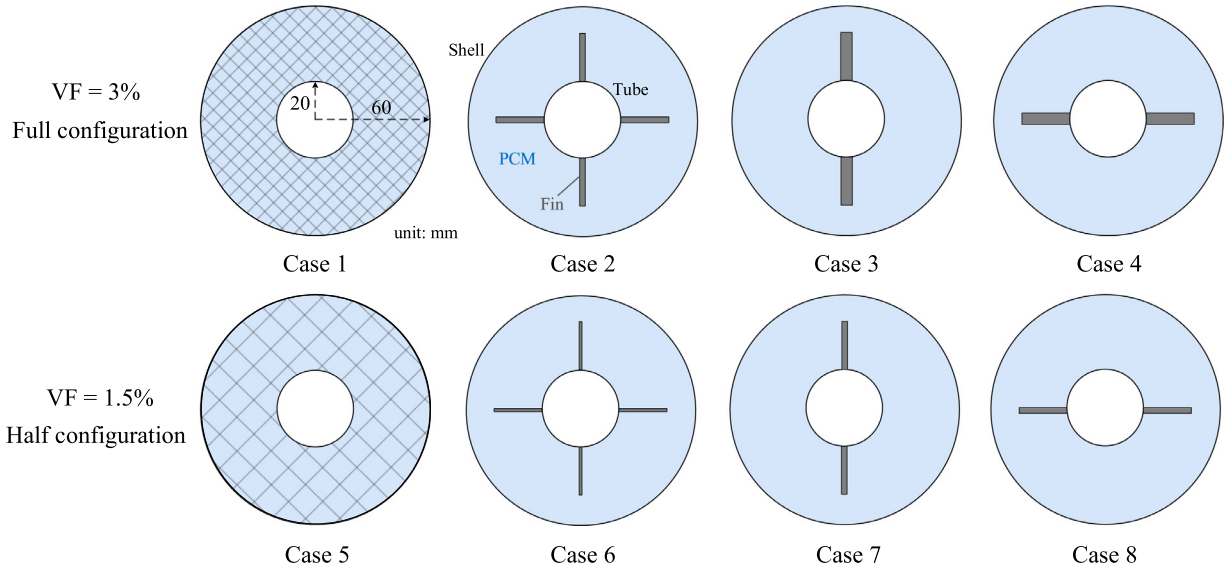

Fig. 1. Schematic of metal foam- and fin-enhanced heat storage units. VF: volume fraction of copper.

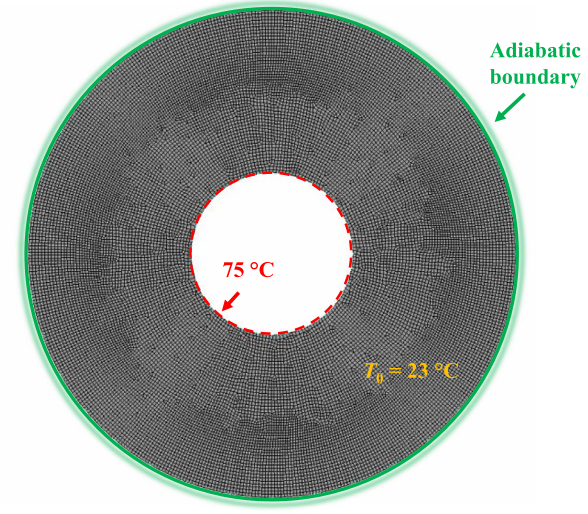

Fig. 2. Schematic of the grid set of 18,831 cells.

Momentum equations for PCM/metal foam composite are given by [22]:

$$\frac{\rho_{\mathrm{PCM}}}{\varepsilon}\frac{\partial u}{\partial t}+\frac{\rho_{\mathrm{PCM}}}{\varepsilon^2}\left(\vec{U}\cdot\nabla u\right) = -\frac{\partial p}{\partial x}-\frac{\mu_{\mathrm{PCM}}}{K}u-\frac{\rho_{\mathrm{PCM}}F_1}{\sqrt{K}}|u|u+\frac{\mu_{\mathrm{PCM}}}{\varepsilon}\nabla^2 u-\frac{(1-\varphi)^2}{(\varphi^3+\omega)}A_{\mathrm{mushy}}u \quad (5)$$

$$\frac{\rho_{\mathrm{PCM}}}{\varepsilon}\frac{\partial v}{\partial t}+\frac{\rho_{\mathrm{PCM}}}{\varepsilon^2}\left(\vec{U}\cdot\nabla v\right) = -\frac{\partial p}{\partial y}-\frac{\mu_{\mathrm{PCM}}}{K}v-\frac{\rho_{\mathrm{PCM}}F_1}{\sqrt{K}}|v|v+\frac{\mu_{\mathrm{PCM}}}{\varepsilon}\nabla^2 v+\rho_{\mathrm{PCM}}\,g\,\beta\left(T-T_{\mathrm{m1}}\right) -\frac{(1-\varphi)^2}{(\varphi^3+\omega)}A_{\mathrm{mushy}}v \quad (6)$$

where ε is the porosity; K is the permeability; and F_1 is the inertia resistance coefficient. The correlations for predicting K and F_1 are as follows [23]:

$$K=\frac{\varepsilon^2\left(d_{\mathrm{fp}}\sqrt{\kappa_{\mathrm{tor}}/3\varepsilon}\right)^2}{36\left(\kappa_{\mathrm{tor}}-1\right)\kappa_{\mathrm{tor}}} \quad (7)$$

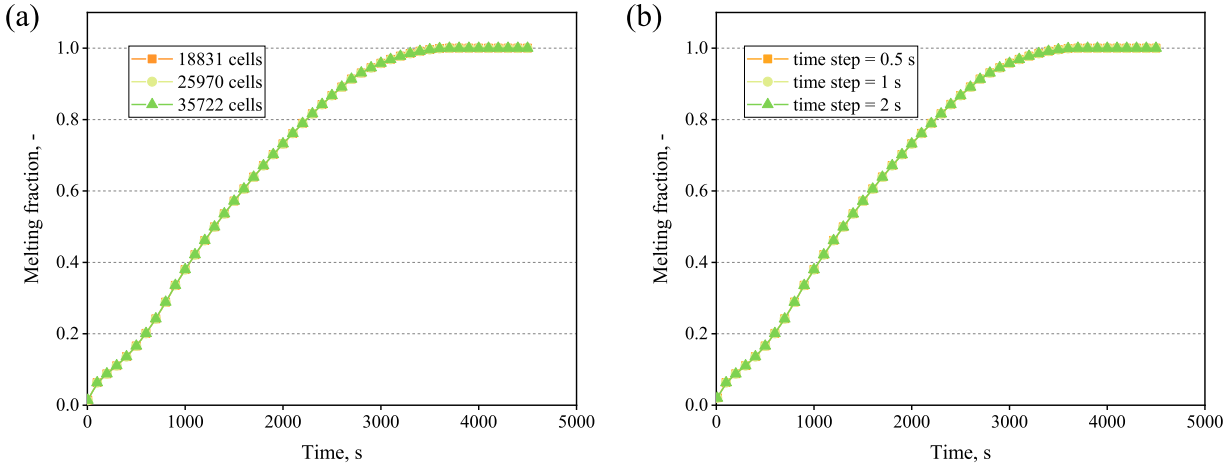

Fig. 3. Variation of melting fraction under different (a) mesh sets and (b) time steps.

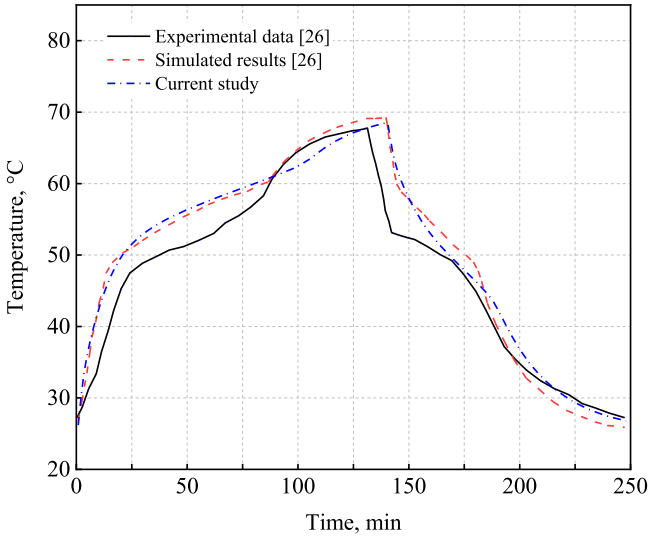

Fig. 4. Validation of the current model with Ref. [26].

$$F_l = 0.00212(1-\varepsilon)^{-0.132}\left(d_{fs}/d_{fp}\right)^{-1.63} \tag{8}$$

$$d_{fp} = \frac{25.4\times10^{-3}}{PPI} \tag{9}$$

$$d_{fs} = 1.18\sqrt{\frac{1-\varepsilon}{3\pi}}\left[\frac{1}{1-e^{(\varepsilon-1)/0.04}}\right] \tag{10}$$

$$\frac{1}{\kappa_{tor}} = \frac{3}{4\varepsilon}+\frac{\sqrt{9-8\varepsilon}}{2\varepsilon}\cos\left\{\frac{4\pi}{3}+\frac{1}{3}\cos^{-1}\left[\frac{8\varepsilon^2-36\varepsilon+27}{(9-8\varepsilon)^{1.5}}\right]\right\} \tag{11}$$

The energy equation for the PCM/fin configuration is shown as follows [20]:

$$\rho_{PCM}\, c_{p,\,PCM}\left(\frac{\partial T}{\partial t}+\vec{U}\cdot\nabla T\right) = k_{PCM}\nabla^2 T-\rho_{PCM}L\frac{d\varphi}{dt} \tag{12}$$

The energy equations for the PCM/metal foam composite are given by [9]:

$$\varepsilon\,\rho_{PCM}\,c_{p,\,PCM}\frac{\partial T_{PCM}}{\partial t}+\varepsilon\,\rho_{PCM}\,c_{p,\,PCM}\left(\vec{U}\cdot\nabla T_{PCM}\right) = k_{ef,\,PCM}\nabla^2 T_{PCM}+h_v\left(T_{ps}-T_{PCM}\right)-\varepsilon\,\rho_{PCM}\,L\frac{df_l}{dt} \tag{13}$$

$$(1-\varepsilon)\rho_{ps}c_{p,\,ps}\frac{\partial T_{ps}}{\partial t} = k_{ef,\,ps}\nabla^2 T_{ps}-h_v\left(T_{ps}-T_{PCM}\right) \tag{14}$$

where c_p is the specific heat, and k_{ef} is the thermal conductivity, which is predicted by Yao et al. [24] model:

$$k_{ef,\,ps} = \frac{1-\varepsilon}{3}k_{ps} \tag{15}$$

$$k_{ef,\,PCM} = \frac{2+\varepsilon}{3}k_{PCM} \tag{16}$$

where k_{ps} and k_{PCM} are the thermal conductivity of porous skeleton and PCM, respectively.

The volumetric interfacial heat transfer coefficient (h_v) is calculated as follows [25]:

$$h_v = \frac{Nu\,k_{PCM}}{d_{fs}^2} \tag{17}$$

$$Nu = \begin{cases} 76.99-152.01\varepsilon+75.04\varepsilon^2 & 0 \le Re \le 0.1 \\ (1.72+1.71\varepsilon-3.46\varepsilon^2)Re^{0.26}Pr^{0.28} & 0.1 < Re \le 1 \end{cases} \tag{18}$$

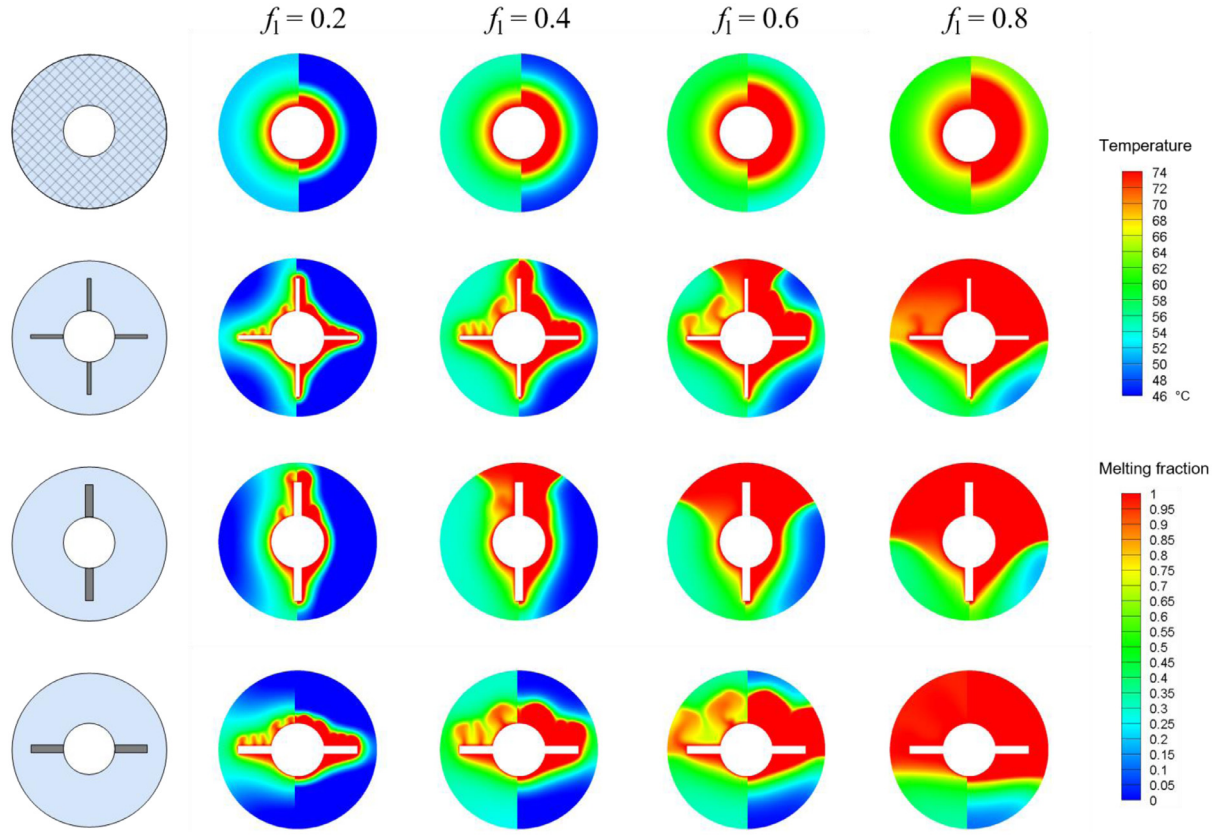

Fig. 5. Melting front propagation (right semicircle) and temperature distribution (left semicircle) for cases 1–4.

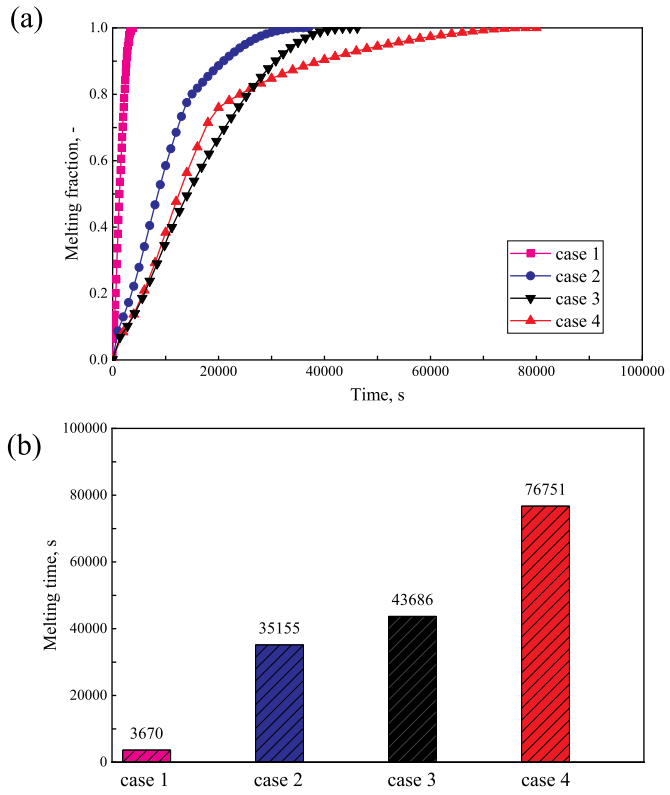

Fig. 6. (a) Variation of melting fraction with time for different cases. (b) total melting time for different cases.

2.2. Initial and boundary conditions

The initial conditions are:

$$T = 23\ ^{\circ}\mathrm{C} \tag{19}$$

The boundary condition for the tube is:

$$T_{\mathrm{tube}} = 75\ ^{\circ}\mathrm{C} \tag{20}$$

The shell is set as adiabatic:

$$\left.\frac{\partial T_{\mathrm{shell}}}{\partial r}\right|_{r=60} = 0 \tag{21}$$

At the interface between the fin and PCM:

$$T_{\mathrm{PCM}} = T_{\mathrm{fin}},\ (-k_{\mathrm{PCM}}\nabla T_{\mathrm{PCM}})\cdot n = (-k_{\mathrm{fin}}\nabla T_{\mathrm{fin}})\cdot n,\ u = v = 0 \tag{22}$$

2.3. Grid and time step independence test

The numerical model was solved using Ansys Fluent. Three mesh sets for case 1 (18,831 cells, 25,970 cells and 35,722 cells) were tested. The schematic of the grid set (18,831 cells) is shown in Fig. 2. The element sizes of three mesh sets are 0.800 mm, 0.068 mm, and 0.058 mm, respectively. The element size had almost no influence on the results (Fig. 3(a)). The grid details for 8 cases used in the simulation are listed in Table 3. Then, three time steps were tested. From Fig. 3(b), the impact of the time step on the melting fraction is low. 25,970 cells and 1 s were adopted in the current research.

Table 3
Grid details for 8 cases.

	Case 1	Case 2	Case 3	Case 4	Case 5	Case 6	Case 7	Case 8
Number of cells	25,970	23,966	24,550	24,538	25,970	24,081	24,582	24,570
Element size (mm)	0.068	0.068	0.068	0.068	0.068	0.068	0.068	0.068

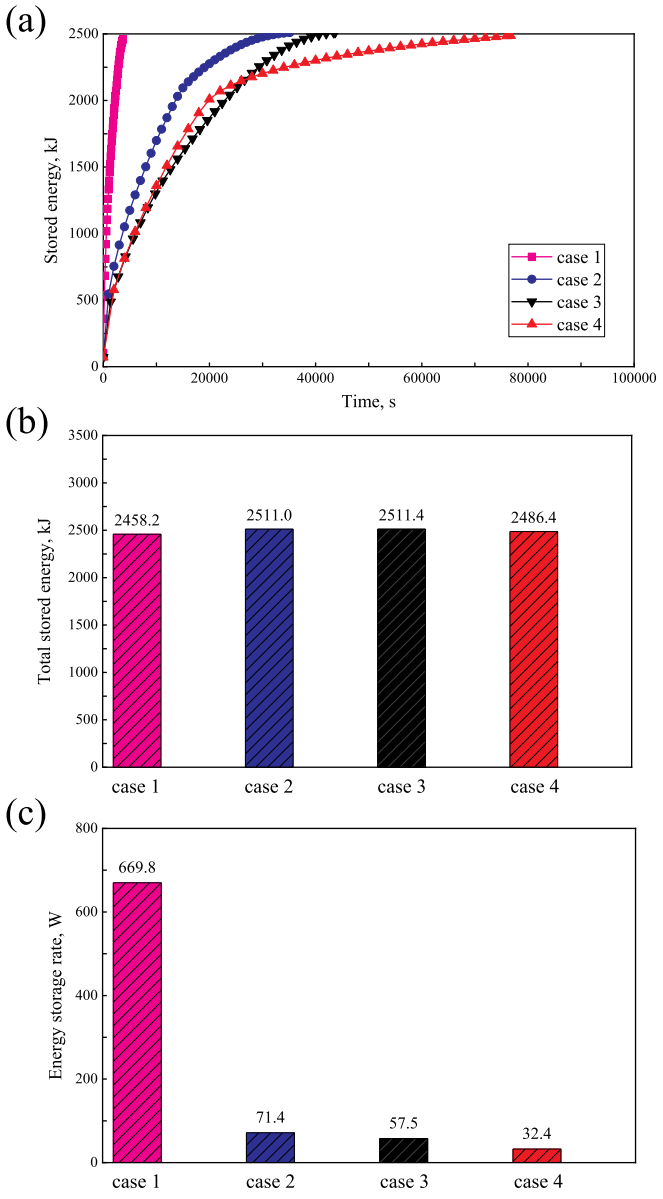

Fig. 7. Variation trend of the stored energy. (a) Variation of stored energy with time, (b) total stored energy for different cases, and (c) energy storage rate for different cases.

2.4. Model validation

Atal et al. [26] researched experimentally the phase change of paraffin in a shell-and-tube unit. Aluminum foam was used as the thermal enhancer. The authors recorded the temperature of a point (configuration: aluminum foam/paraffin, 0.95 porosity). The results are shown in Fig. 4 [26]. In addition, the authors performed a numerical simulation and predicted the temperature evolution. The same geometry and thermo-physical properties were employed in the current study. Fig. 4 presents the experimental and simulated results. At 0–25 min, the simulated results are higher than the experimental results. This is because it is assumed that the boundary is adiabatic in the simulation, while there can be some heat loss in the experiment. After 70 min, the melting is finished. The difference between the experimental and numerical values decreases; the experimental values are higher than the numerical values at the last stage. This is because in the simulation, the specific heat of the liquid paraffin and solid paraffin is set the same;

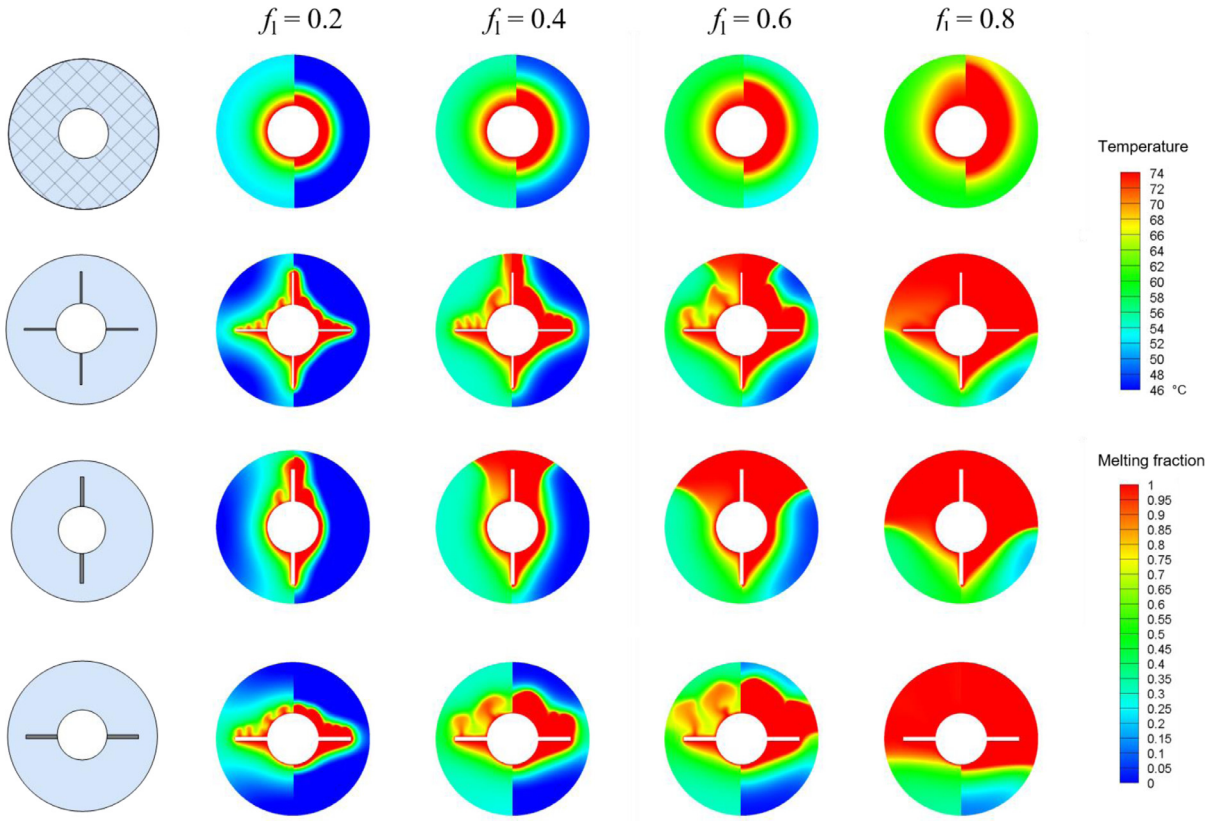

Fig. 8. Melting front propagation (right semicircle) and temperature distribution (left semicircle) for cases 5–8.

in reality, the former is lower than the latter [23]. The maximum deviation is 13.4 ˚C (19.7%) when the solidification process starts in the simulation (114 min), after which the discrepancy decreases. The simulated and experimental results are almost the same at the final stage. Compared to the simulated results reported by Atal et al. [26], the deviation is less than 4%. Therefore, the current numerical model is feasible.

3. Results and discussions

3.1. Full configuration

The melting front propagation and temperature distributions are shown in Fig. 5. For case 1, the melting is homogenous. The melting rate of the upper half is almost the same as that of the lower half. For case 2, at $f_l = 0.2$, the solid-liquid interface is symmetric; the PCM near the fins is melted first. Subsequently, the upper half part has a faster melting rate than the lower counterpart. The liquid and hot PCM flows upward under the buoyancy force, accelerating the melting in the upper half part. Cases 3 and 4 show a similar phenomenon. In case 1, the metal foam suppresses the natural convection, which should lead to a homogeneous solid-liquid interface.

Fig. 6(a) shows the variation of the melting fraction for the 4 cases. For case 1, the melting fraction increases the most rapidly. The following one is case 2. The melting fraction of case 3 initially increases less rapidly than case 4, but the overall melting rate is faster than case 4. This may be attributed to the vertical fin accelerating the melting of PCM in the lower part. From Fig. 5, the melting in the lower part is obviously slower than that in the upper part. In case 3, the PCM near the lower vertical fin melts fast. By contrast, in case 4, the PCM at the lower part, particularly at the bottom, is hardly affected by the horizontal fins.

The melting time of case 1 is the shortest, followed by case 2, case 3, and case 4. These results indicate that metal foam has the best heat transfer enhancement performance, and that 4 fins are superior to two fins.

Fig. 7 indicates that the stored energy has a similar variation trend to the melting rate. The total stored energy for 4 cases is nearly identical, and a slight difference should result from the sensible heat energy. Case 1 has the highest energy storage rate, which is 20 times higher than that of case 4.

3.2. Half configuration

The melting front propagation and temperature distribution for cases 5–8 are shown in Fig. 8. For case 5, the phase interphase is almost the same as in case 1, except at $f_l = 0.8$, where the melt front is egg-shaped. This is because the flow resistance becomes weak owing to the higher porosity in case 5, resulting in stronger natural convection. The melting front propagation and temperature distribution for case 6 is similar to that of case 2. The condition is the same for case 7 and case 8.

Fig. 9(b) shows that the total melting time of case 5 is 7,242 s, which is 97.3% longer than that of case 1. For cases 6–8, the variation of the melting fraction does not vary significantly from those of cases 2–4. In addition, the total melting time is only slightly increased. This is because the contact area between fins and PCM decreased marginally. Overall, the half configuration has a significant effect on the metal foam-enhanced unit, while it hardly affects the fin-enhanced units.

The stored energy and the melting fraction have the same variation trend (Fig. 10). Case 5, i.e., the metal foam-enhanced unit, has the highest energy storage rate, followed by case 6, case 7, and case 8. The energy storage rate for case 5 is 10 times higher than that for case 8. Although the energy storage rate of the metal foam-enhanced unit is significantly decreased, it is still the highest one.

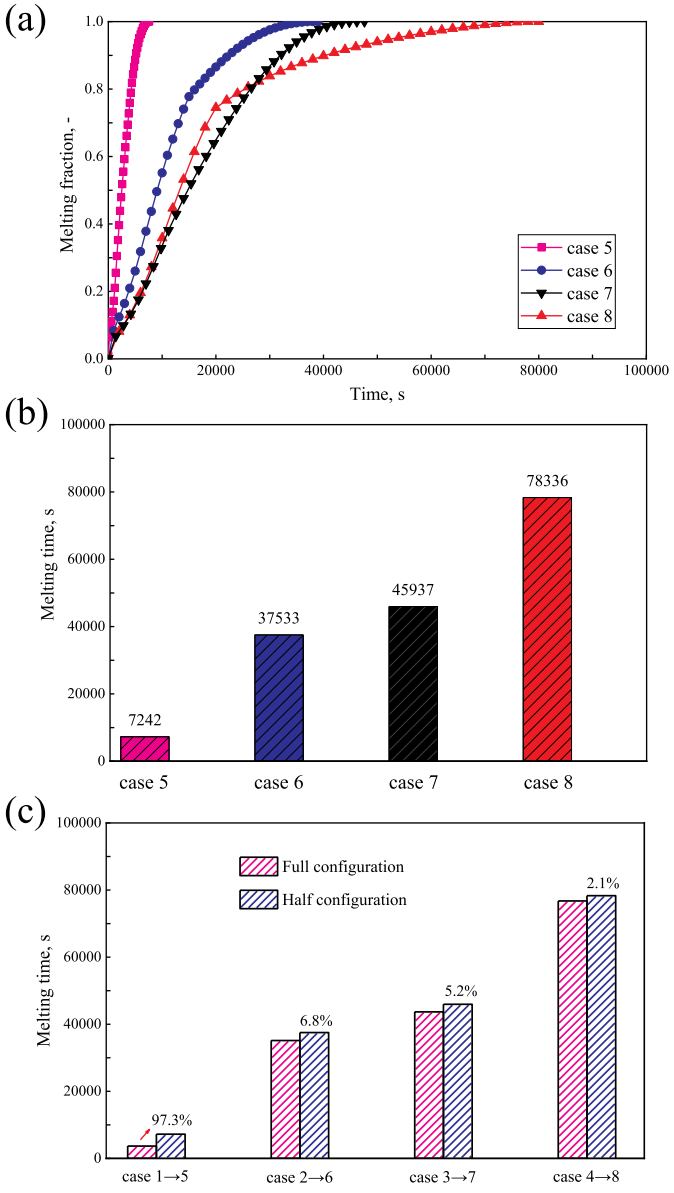

Fig. 9. (a) Variation of melting fraction with time, (b) total melting time for cases 5–8, and (c) comparison of the melting time of the full configuration and the half configuration.

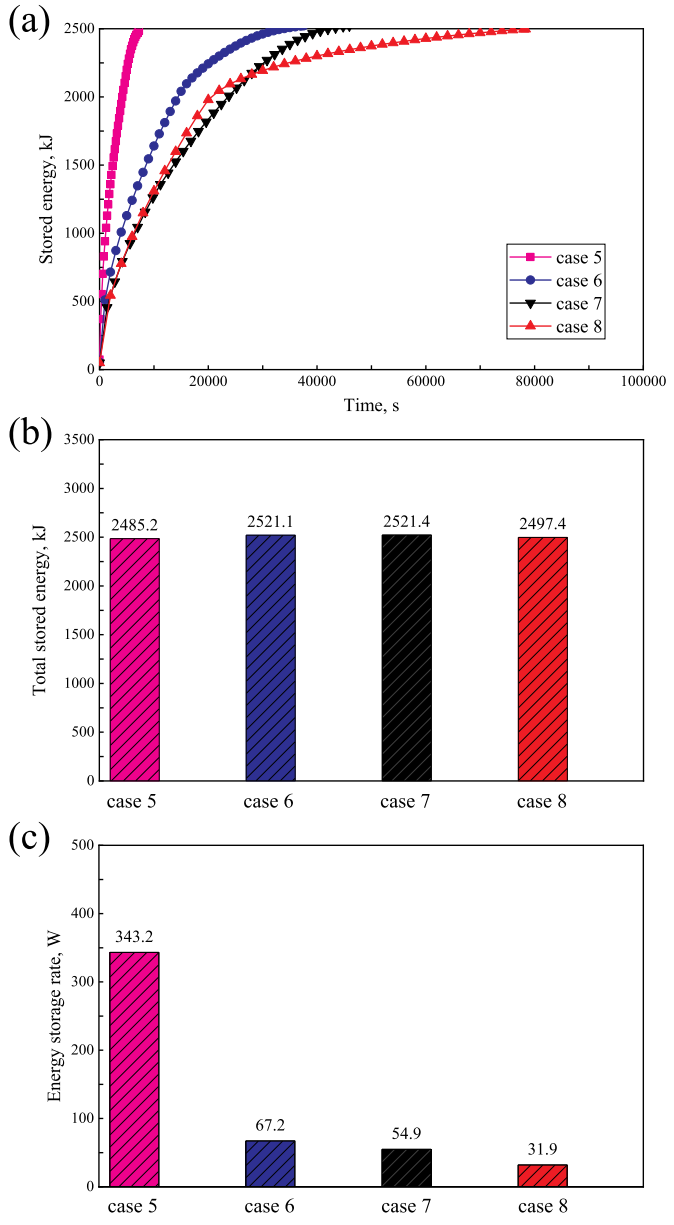

Fig. 10. (a) Variation of stored energy with time, (b) total stored energy for different cases, and (c) energy storage rate for difference cases.

4. Conclusions

In the current study, two popular thermal enhancers, i.e., metal foam and fins, are compared to provide guidance on the choice of the optimal structure for practical applications. Three fin structures (four fins, two vertical fins, and two horizontal fins) are included, and the following conclusions are made:

(1) For the full configuration (volume fraction of metal = 3%), the melting rate in the unit with four fins is faster than the one with vertical or horizontal fins. In other words, increasing the number of fins helps to accelerate melting. Horizontal fins have the weakest enhancement performance, and metal foam exhibits the best enhancement performance. The energy storage rate in the unit with metal foam is approximately 20 times higher than that in the unit with horizontal fins. The four cases have nearly the same total stored energy.

(2) For the half configuration (volume fraction of metal = 1.5%), the solid-liquid phase interface as well as the temperature field is similar to that under the full configuration. The total melting time in the unit with metal foam almost doubles, while there is no remarkable change in the units with fins. Nevertheless, metal foam still exhibits the best enhancement performance. The energy storage rate in the unit with metal foam can be up to 10 times higher than that of the fin-enhanced unit.

Declaration of competing interest

The authors declare that there are no conflicts of interest.

Acknowledgments

This work was supported by the National Key R&D Program of China (Grant No.: 2018YFA0702300), H2020-MSCA-RISE-778104-ThermaSMART, and the Doctoral Degree Scholarship offered by the China Scholarship Council (CSC).

References

[1] S.A. Mohamed, F.A. Al-Sulaiman, N.I. Ibrahim, et al., A review on current status and challenges of inorganic phase change materials for thermal energy storage systems, Renew. Sust. Energ. Rev. 70 (2017) 1072–1089.

[2] S. Zhang, Z. Li, Y. Yao, et al., Heat transfer characteristics and compatibility of molten salt/ceramic porous composite phase change material, Nano Energy 100 (2022) 107476.

[3] M. Liu, W. Saman, F. Bruno, Review on storage materials and thermal performance enhancement techniques for high temperature phase change thermal storage systems, Renew. Sust. Energ. Rev. 16 (2012) 2118–2132.

[4] S. Zhang, Y. Yan, Energy, exergy and economic analysis of ceramic foam-enhanced molten salt as phase change material for medium- and high-temperature thermal energy storage, Energy 262 (2023) 125462.

[5] Z. Li, X. Yu, L. Wang, et al., Effects of fluctuating thermal sources on a shell-and-tube latent thermal energy storage during charging process, Energy 199 (2020) 117400.

[6] N.I. Ibrahim, F.A. Al-Sulaiman, S. Rahman, et al., Heat transfer enhancement of phase change materials for thermal energy storage applications: a critical review, Renew. Sust. Energ. Rev. 74 (2017) 26–50.

[7] Q. Li, C. Li, Z. Du, et al., A review of performance investigation and enhancement of shell and tube thermal energy storage device containing molten salt based phase change materials for medium and high temperature applications, Appl. Energ. 255 (2019) 113806.

[8] S. Zhang, Y. Yan, Thermal performance of latent heat energy storage system with/without enhancement under solar fluctuation for Organic Rankine power cycle, Energ. Convers. Manage. 270 (2022) 116276.

[9] Y. Xu, Q. Ren, Z.-J. Zheng, et al., Evaluation and optimization of melting performance for a latent heat thermal energy storage unit partially filled with porous media, Appl. Energ. 193 (2017) 84–95.

[10] Z. Liu, Y. Yao, H. Wu, Numerical modeling for solid–liquid phase change phenomena in porous media: shell-and-tube type latent heat thermal energy storage, Appl. Energ. 112 (2013) 1222–1232.

[11] X. Yang, P. Wei, X. Wang, et al., Gradient design of pore parameters on the melting process in a thermal energy storage unit filled with open-cell metal foam, Appl. Energ. 268 (2020) 115019.

[12] X. Yang, P. Wei, X. Cui, et al., Thermal response of annuli filled with metal foam for thermal energy storage: an experimental study, Appl. Energ. 250 (2019) 1457–1467.

[13] E. Fleming, S. Wen, L. Shi, et al., Experimental and theoretical analysis of an aluminum foam enhanced phase change thermal storage unit, Int. J. Heat. Mass. Tran. 82 (2015) 273–281.

[14] M.A. Dekhil, J.V. Simo Tala, O. Bulliard-Sauret, et al., Numerical analysis of the performance enhancement of a latent heat storage shell and tube unit using finned tubes during melting and solidification, Appl. Therm. Eng. 192 (2021) 116866.

[15] R. Ge, Q. Li, C. Li, et al., Evaluation of different melting performance enhancement structures in a shell-and-tube latent heat thermal energy storage system, Renew. Energ. 187 (2022) 829–843.

[16] C. Zhang, J. Li, Y. Chen, Improving the energy discharging performance of a latent heat storage (LHS) unit using fractal-tree-shaped fins, Appl. Energ. 259 (2020) 114102.

[17] Z. Liu, Z. Liu, J. Guo, et al., Innovative ladder-shaped fin design on a latent heat storage device for waste heat recovery, Appl. Energ. 321 (2022) 119300.

[18] P. Zhang, Z.N. Meng, H. Zhu, et al., Melting heat transfer characteristics of a composite phase change material fabricated by paraffin and metal foam, Appl. Energ. 185 (2017) 1971–1983.

[19] S. Zhang, Y. Yao, Y. Jin, et al., Heat transfer characteristics of ceramic foam/molten salt composite phase change material (CPCM) for medium-temperature thermal energy storage, Int. J. Heat. Mass. Tran. 196 (2022) 123262.

[20] M. Caliano, N. Bianco, G. Graditi, et al., Analysis of a phase change material-based unit and of an aluminum foam/phase change material composite-based unit for cold thermal energy storage by numerical simulation, Appl. Energ. 256 (2019) 113921.

[21] S. Zhang, D. Feng, L. Shi, et al., A review of phase change heat transfer in shape-stabilized phase change materials (ss-PCMs) based on porous supports for thermal energy storage, Renew. Sust. Energ. Rev. 135 (2021) 110127.

[22] Z.G. Qu, W.Q. Li, W.Q. Tao, Numerical model of the passive thermal management system for high-power lithium ion battery by using porous metal foam saturated with phase change material, Int. J. Hydrogen Energy 39 (2014) 3904–3913.

[23] Y. Yao, H. Wu, Macroscale modeling of solid–liquid phase change in metal foam/paraffin composite: effects of paraffin density treatment, thermal dispersion, and interstitial heat transfer, J. Therm. Sci. Eng. Appl. 13 (2021) 041024.

[24] Y. Yao, H. Wu, Interfacial heat transfer in metal foam porous media (MFPM) under steady thermal conduction condition and extension of Lemlich foam conductivity theory, Int. J. Heat. Mass. Tran. 169 (2021) 120974.

[25] Y. Yao, H. Wu, Z. Liu, Direct simulation of interstitial heat transfer coefficient between paraffin and high porosity open-cell metal foam, J. Heat Transfer 140 (2018) 032601.

[26] A. Atal, Y. Wang, M. Harsha, et al., Effect of porosity of conducting matrix on a phase change energy storage device, Int. J. Heat. Mass. Tran. 93 (2016) 9–16.